Image Selection Based on Grayscale Features in Robotic Welding

Zhen Ye[1,2], Gu Fang[1], Shanben Chen[2], and Ju Jia Zou[1]

[1] School of engineering, University of Western Sydney, Australia, 2751
17191207@student.uws.edu.au, {G.Fang,J.Zou}@uws.edu.au
[2] Institute of Welding Engineering, Shanghai Jiao Tong University, China, 200240
{ruan,sbchen}@sjtu.edu.cn

Abstract. In robotic welding seam tracking based on visual information has been studied in the recent years. However, it is difficult to ensure the quality of images obtained in the welding process because it is easily affected by spattering, fuming and electromagnetic noise. The paper introduces a method to select useful images before further processing. Experimental tests are conducted to verify its accuracy.

Keywords: Pulsed MIG, Vision Sensor, Image selection, Grayscale.

1 Introduction

Currently, most of the robots used in arc welding applications are of the "teach and playback" type. However, such robotic welding systems are rigid and cannot adjust to errors in the weld seam coordinates caused by natural welding environmental factors. Therefore sometimes these robotic welders cannot meet the high quality requirement of the welding process. To address this issue, some seam tracking systems are developed to solve the problem [1-6]. In these systems, visual sensors have been adopted because of their non-contact to the weld pool and rich information of the welding process. In some studies [7-9], camera was designed with filters to view the welding process directly. This direct observation of the welding process helped to realize the seam tracking based on the size and the position of the seam and the welding pool. However, it is difficult to ensure that welding images obtained during the welding process are clear and contain useful information. Furthermore, welding images are more easily spoiled in MIG welding due to its less stable process than the TIG welding.

In this paper, a method is developed to select images based on image's grayscale and histogram features. This selection process will allow only those images deemed 'useful' to be further processed. This selection process not only avoids the unnecessary image processing, but also provides reference for future adaptive edge detection.

The rest of this paper is organized as follows: the robotic welding system used in image acquisition is described in Section 2. In section 3, a method to select images is developed and in Section 4 a series of tests are conducted to confirm the effectiveness and accuracy of the method. Finally, Section 5 summarizes the finding of the paper.

H. Deng et al. (Eds.): AICI 2011, Part III, LNAI 7004, pp. 63–70, 2011.

2 The Experiment System

The welding robot system in our research includes a “teach and playback” robot, a visual sensor composed of a CCD camera and the optical filters, a current sensor, welding source and a computer. The schematic diagram of the system is shown in Fig.1.

Q235 steel sheet is welded by pulsed MIG welding. And shielding gas is 92% Ar +8% CO_2. Some other welding conditions are listed in Table 1.

Table 1. Welding parameters

Groove type	Wall thickness	Diameter of welding wire	Root gap	Root face	Welding current	welding voltage	Flow rate	Wire feed rate	Welding speed
V	4.5mm	1.2mm	0	1mm	146A	25V	15L/min	4m/min	5mm/s

By performing the spectrum analysis of the welding scenes under the above welding conditions, it is found that the light spectrum from 620nm to 680nm is composed of continuous line, and the intensity of this light spectrum is lower than others. Consequently an optical filter is chosen with the central wavelength of 660nm. Furthermore, a dimmer glass is also selected for the visual sensor to reduce the exposure light going into the camera. Another factor that affects the quality of the image is the welding current [10]. Therefore the image capturing is controlled to take place when the welding current is at its minimum.

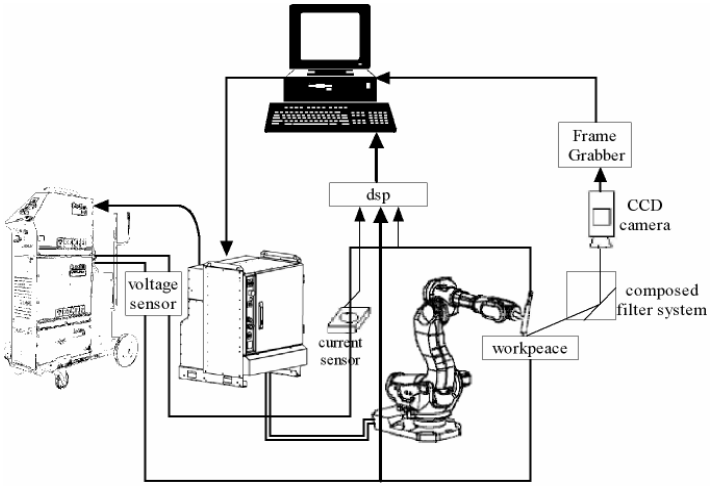

Fig. 1. The schematic diagram of the welding robot system

3 A Method for Image Selection

Since welding images are affected by droplet transfer, spattering, fuming and electromagnetic noise, it is difficult to ensure that every image captured is clear even

when we control the capturing moment. Processing an image without useful information not only is a waste of time but also could potentially lead to wrong results being derived. Therefore, an easy and fast method is required to determine which images are 'useful' for further processing.

According to the analysis of images, they can be divided into three classes: dark, good, and bright. The criteria to discriminate these classes are shown in Table 2, and typical images in these categories are shown in Figure 2.

Table 2. The criteria for discriminating images

Dark	Brightness is too low and edge of the groove, electrode or welding pool cannot be seen clearly.
Good	Brightness is appropriate and edge of the groove, electrode and welding pool can all be seen clearly.
Bright	Brightness is too high and edge of the groove, electrode or welding pool cannot be seen clearly.

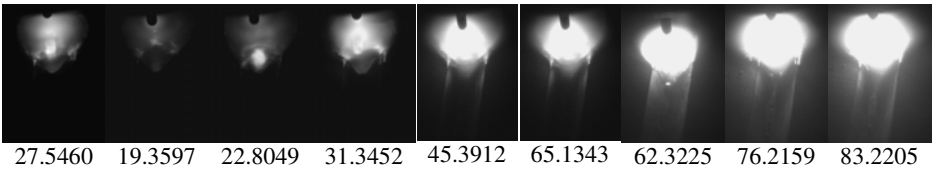

27.5460 19.3597 22.8049 31.3452 45.3912 65.1343 62.3225 76.2159 83.2205

a. Dark **b. Good** **c. Bright**

Fig. 2. Three classes of images (numbers under the images are the average grayscale value of each image): a. Dark. b. Good. c. Bright

3.1 Average Gray Value

The biggest difference between these three classes of images is the variety of their brightness, which can be represented by average gray value as shown in Equation (1).

$$Agv = \frac{\sum_{x=1,y=1}^{x=m,y=n} f(x,y)}{m \times n} \tag{1}$$

Where:

Agv is the Average Gray Scale Value of the image;
f(x,y) is the pixel value of the xth row and the yth column in an image;
m is the number of rows in an image;
n is the number of columns in an image.

The average gray scale values of images in Fig 2 are shown under each image. During the experiments, 350 images were captured. Amongst these, 70 are regarded as dark images, 200 are good images and 80 are bright images as determined by

human observation. To develop the image selection method, we used half of these images, i.e., 35 dark images, 100 good images and 40 bright images to determine the selection criteria. The rest of them are used to test the accuracy of our selection method.

By analyzing average gray scale values of three classes of images, the threshold of Agv is acquired, as shown in Table 3.

Table 3. The threshold of the average grayscale value

Class	Average gray value
Dark	Agv≤30
Good	39≤Agv≤60
Bright	Agv>70

It can be seen from the figures in Table 3 that there are gaps between 30 ~ 39 and 60 ~ 70. In these gaps, the images cannot be classified correctly. This is because there are both Dark and Good images with Agvs between 30 and 39 and Good and Bright images with Agvs between 60 and 70. This 'overlap' phenomenon could be shown in Fig 3. Thus additional criterion is needed.

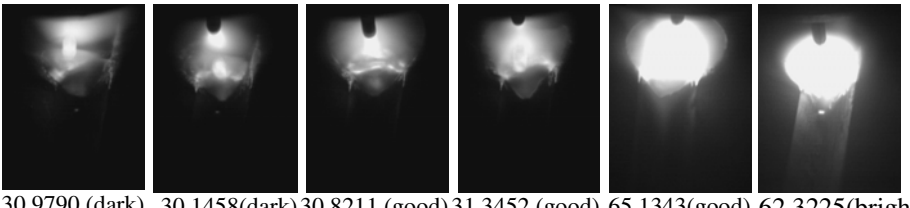

30.9790 (dark) 30.1458(dark) 30.8211 (good) 31.3452 (good) 65.1343(good) 62.3225(bright)

a **b** **c** **d** **e** **f**

Fig. 3. The images which cannot be discriminated easily

3.2 Histogram Features

By analyzing Figure 3.a~b and Figure 3.c~d, it is found that the biggest difference between them is the clarity of the weld seam. So the area occupied by the seam is separated from the original image, and its average gray value is calculated, as shown in Fig 4. However, the result shows that it is impossible to discriminate them in this way.

According to these images, the intensity of the arc light has a great impact on the definition of the seam. Therefore features of the arc light can indirectly affect the clarity of the seam. Observing the pixel values around the weld zone, it is found that the different ranges of their magnitude reflect corresponding parts of the welding image. A typical image and its grayscale distribution are shown in Figure 5.

19.7961 (dark) **a** | 18.1087 (dark) **b** | 19.8893(good) **c** | 19.6322(good) **d**

Fig. 4. The seams of the images in Fig. 3.a~d and their average gray values

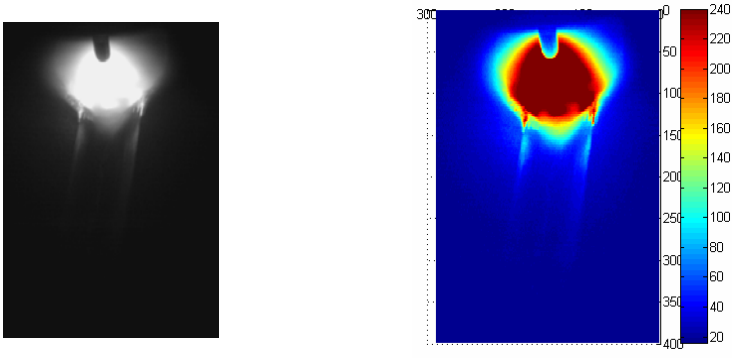

Fig. 5. A typical welding image and its grayscale distribution

From Figure 5 it is clear that the arc light mainly contains the pixels on the range of gray value from 235 to 240, and the area that arc light may influence has the pixel intensity value from 180 to 240. Therefore, this range of 180 to 240 is a good representation of the arc light. To count the area with this 'good lighting' conditions, Equation 2 is developed.

$$g(x,y)=\begin{cases}1 & 180\le f(x,y)\le 240\\ 0 & others\end{cases}$$
$$IAR=\sum_{x=1,y=1}^{x=m,y=n} g(x,y) \tag{2}$$

Where:

IAR is the area that arc light may influence and g(x,y) is the modified intensity of the pixel. All other notations are the same as those in Equation 1.

However, this measure will fail when the object of the camera is moving faster, which could enlarge the area of the range from 180 to 240 and reduce that of the range from 235 to 240. Therefore, it is worthwhile to count the intensity contents in the range of 235 to 240. This measure is calculated using Equation 3.

$$g(x,y)=\begin{cases}1 & 235\le f(x,y)\le 240\\ 0 & others\end{cases}$$
$$AL=\sum_{x=1,y=1}^{x=m,y=n} g(x,y) \tag{3}$$

where:

AL is the area of the arc light. All other notations are the same as those in Equation 2.

It is found, by the analysis of the Figure 3.e~f, that the biggest distinction between them is the clarity of the welding pool. Since the gray value of the welding pool is quite different from that of the arc light, we can use this difference to discriminate this situation. From Figure 5 it is observed that the welding pool mainly contains pixels on the range of gray value from 100~180. Therefore, Equation 4 is developed to count the welding pool area in the image.

$$g(x,y)=\begin{cases}1 & 100\le f(x,y)\le 180\\ 0 & others\end{cases}$$
$$WPL=\sum_{x=1,y=1}^{x=m,y=n} g(x,y) \tag{4}$$

Where:

WPL is the welding pool area where gray values range from 100~180. All other notions are the same as those in Equations 2 and 3.

The selection criteria that incorporate all three measures expressed in equations 2 – 4 are shown in Tables 5 and 6.

Table 4. Threshold of AL and IAR

Class	Criteria
Good	IAR>1400 && AL>600
Dark	Others

Table 5. Threshold of WPL

Class	Criteria
Good	WPL>6000
Bright	Others

3.3 Selection of Images

By combining the selection criteria presented above, the overall selection process is done as:

- Calculating the average gray value of the image and classifying it by Table 3;
- If the AGV of the image is among 30~39, IAR and AL should be calculated and the image is classified by Table 4.
- If the AGV of the image is among 60~70, WPL should be calculated and the image is classified by Table 5.

4 Results and Discussions

The method developed in Section3 is used to recognize the remaining 175 images, and the results are shown in Table 7.

Table 6. The result of recognition

Recognition Results / Human observation results	Dark	Good	Bright	Recognition Accuracy
Dark	35	1	0	97.2%
Good	0	96	4	96%
Bright	0	2	38	95%

From Table 7, it can be seen that the images are being selected with an accuracy rate of more than 95%. Although misjudgements still occur occasionally, the situations that lead to these misjudgements are discussed below.

Dark images are judged as Good ones
In some images, droplets cover a part of arc light, as shown in Figure 6.a. It happens to affect the arc light as a source for the seam. However, it does not have a great impact on IAR.

Good images are judged as Bright ones
Sometimes the edge of the arc light and that of the welding pool almost coincide, as shown in Figure 6.b. This results in WPL smaller than normal, and causes mistakes.

Bright images are recognized as Good ones
This happens when the arc deviates from the centre of the welding pool, as shown in Figure 6.c. From the image, a side of the welding pool can be seen clearly, therefore the image meet the criteria in section 3.2. However, the other side is covered by the deviated arc, which leads to an incomplete welding pool and therefore makes the information useless.

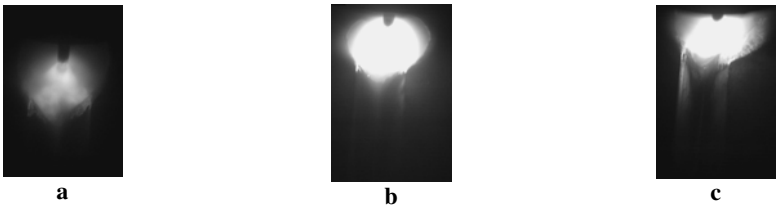

Fig. 6. Images which is misjudged

Overall, the probability of misjudgment due to situations discussed above is very small, less than 5% Therefore, the method provided in this paper is effective for image selection.

5 Conclusion

The paper defines three general classes of images in the welding process. To select good images, the paper analyzes the relationship between images and their gray scale distributions, and finds that average gray value and histogram features can be used to discriminate images. A method is developed to select Good images using these criteria. It is found using experiments that the recognition accuracy is above 95%.

Acknowledgement. This work is partly supported by the Australian Research Council under project ID LP0991108 and the Lincoln Electric Company (Australia).

References

1. Kim, J.W., Na, S.J.: Study on arc sensor algorithm for weld seam tracking in gas metal arc welding of butt joints. In: Proceedings of the Institution of Mechanical Engineers, Part B: Journal of Engineering Manufacture, vol. 205(B4), pp. 247–255 (1991)
2. Suga, Y., Naruse, M., Tokiwa, T.: Application of neural network to visual sensing of weld line and automatic tracking in robot welding. Welding in the World 34, 275–282 (1994)
3. Kuo, H.-C., Wu, L.-J.: An image tracking system for welded seams using fuzzy logic. J. Mater. Process. Technol. 120(1), 169–185 (2000)
4. Lee, S.K., Na, S.J.: A study on automatic seam tracking in pulsed laser edge welding by using a vision sensor without an auxiliary light source. J. Manuf. Syst. 21(4), 302–315 (2002)
5. Lee, S.K., Chang, W.S., Yoo, W.S., Na, S.J.: A tudy on a vision sensor based laser welding system for bellows. J. Manuf. Syst. 19(4), 249–255 (2007)
6. Micallef, K., Fang, G., Dinham, M.: Automatic Seam Detection and Path Planning in Robotic Welding. In: Tarn, T.J., Chen, S.B., Fang, G. (eds.) Robotic Welding, Intelligence and Automation, pp. 23–32. Springer, Heidelberg (2011)
7. Bae, K.Y., Lee, T.H., Ahn, K.C.: An optical sensing system for seam tracking and weld pool control in gas metal arc welding of steel pipe. J. Mater. Process. Technol. 120(2), 458–465 (2002)
8. Shen, H.Y., Li, L.P., Lin, T., Chen, S.B.: Real-time Seam Tracking Technology of Welding Robot with Visual Sensing. Journal of Intelligent and Robotic systems 59, 283–298 (2010)
9. Ma, H., Wei, S., Sheng, Z.: Robot welding seam tracking method based on passive vision for thin plate closed-gap butt welding. International Journal of Advanced Manufacturing Technology 48, 945–953 (2010)
10. Yan, Z.H., Zhang, G.J., Gao, H.M., Wu, L.: Weld pool boundary and weld bead shape reconstruction based on passive vision in P-GMAW. China Welding 15(2), 20–24 (2006)